Molecular Crystals and Liquid Crystals

Publication details, including instructions for authors and subscription information:
http://www.tandfonline.com/loi/gmcl20

Nematic Braids: Modeling of Colloidal Structures

Miha Ravnik [a], Brina Črnko [a] & Slobodan Žumer [a b]

[a] Faculty of Mathematics and Physics, University of Ljubljana, Ljubljana, Slovenia

[b] Jozef Stefan Institute, Ljubljana, Slovenia

Version of record first published: 05 Oct 2009

To cite this article: Miha Ravnik, Brina Črnko & Slobodan Žumer (2009): Nematic Braids: Modeling of Colloidal Structures, Molecular Crystals and Liquid Crystals, 508:1, 150/[512]-162/[524]

To link to this article: http://dx.doi.org/10.1080/15421400903060532

Mol. Cryst. Liq. Cryst., Vol. 508, pp. 150/[512]–162/[524], 2009

ISSN: 1542-1406 print/1563-5287 online
DOI: 10.1080/15421400903060532

Nematic Braids: Modeling of Colloidal Structures

Miha Ravnik[1], Brina Črnko[1], and Slobodan Žumer[1,2]
[1]Faculty of Mathematics and Physics, University of Ljubljana, Ljubljana, Slovenia
[2]Jozef Stefan Institute, Ljubljana, Slovenia

Our recent advances in modeling of colloidal superstructures in spatially confined nematic liquid crystals are briefly reviewed. The approach is phenomenological and is based on Landau- de Gennes type free energy, where the effects of confinement and external fields are also taken into account. The inter-particle couplings that result in a nematic solvent are effectively many-body interactions. The complexity of the couplings leads to numerous nematic and colloidal structures not present in simple liquids where van der Waals and electrostatic interactions are dominant. A local "heating" to the isotropic phase is performed, followed by a fast quench to the nematic phase. In the relaxation process that conserves the topological charge, a number of metastable colloidal superstructures are formed. Here we focus our attention on the entangled structures where colloidal particles are coupled by an entangled network of delocalized disclination lines (nematic braid): colloidal dimers, chains, and multiscale structures. The string-like coupling provided by such disclination lines is much more robust compared to an interaction based on an array of localized disclinations. The controlled formation of entangled colloidal structures opens new ways to the assembly of colloidal photonic crystals and hierarchical structures that could lead to metamaterials.

Keywords: colloid; disclination; entanglement; hierarchical structure; nematic braid; nematic liquid crystal

PACS Numbers: 61.30.Jf; 47.57.J-; 83.10.Pp

I. INTRODUCTION

Liquid crystal colloids have recently attracted a lot of attention by their combined solid and liquid-like behavior, which enables formation

Authors acknowledge funding from Slovenian Research Agency ARRS (Pl-0099 program).

Address correspondence to Slobodan Žumer, Faculty of Mathematics and Physics, University of Ljubljana, Jadranska 19, Ljubljana SI-1000, Slovenia. E-mail: slobodan.zumer@fmf.uni-lj.si

of structures with new optical and material properties. Focusing on nematic solvents one finds that by introducing anisotropic mesophases, one does not only alter the optical properties of such systems, but also allows new means to assemble regular and complex optical structures. Orientational order of the nematic liquid crystals is usually described by a unit vector field $\boldsymbol{n}$, called the director, with orientations $\boldsymbol{n}$ and $-\boldsymbol{n}$ being indistinguishable [1]. Colloidal particles typically interact with nematic molecules through their surfaces yielding strong spatial variations and even discontinuities in the director field. Areas where the director cannot be defined are called defects. Particles whose surfaces favor perpendicular (homeotropic) orientation are accompanied either by -1 hyperbolic point defects or $-1/2$ disclination loops (Saturn rings) [1–3]. Coupling between the nematic liquid crystal and the inclusion gives rise to an effective field, which acts between the inclusions and can be used for the assembly. The symmetry and the type of defects which accompany colloidal particles prove to be the decisive factor governing the anisotropy and spatial dependence of the effective nematic elastic forces. In the long distance limits the two particles with -1 point defects interact through a $1/r^3$ potential [3], particles with Saturn rings as $1/r^5$ [3] and particles with boojums as $1/r^5$, r being the distance between the particles [4,5]. These different power-laws, together with the anisotropy of the interaction potential profiles, lead to self-assembly of a large variety of colloidal structures, such as chains [2,6], clusters [7] and 2D crystals [8,9]. The inter-particle potential is typically very strong (1000kT for a micrometer particle), and also highly anisotropic, which is a direct consequence of the nematic anisotropy and its long-range orientational order. The recently discovered entangled structures on micron and supramicron exhibit an order of magnitude higher inter-particle potentials [10,11]. The most recent studies showed that topological and elastic properties of liquid crystals could be used to hierarchically self-assemble particles of very different sizes into colloidal superstructures [12].

In this overview our recent achievements in modeling of colloidal structures in nematic liquid crystalline solvents are described. For particles with sizes ranging from few 10 nanometers to few micrometers, the phenomenological approach based on the nematic Landau-de Gennes free energy is particularly useful. Most of the attention will be given to the phenomenon of the entanglement by disclination lines [11]. Three basic entangled defect structures, able to topologically arrest homeotropic colloidal dimmers, will be discussed in detail: figure of eight, figure of omega, and entangled point defect structure. Topological limitations, numerical procedures, and details needed to generate, model, and visualize possible structures will be

described. More complex arrangements of particles, such as chains and multiscale structures will be mentioned. The ability of a liquid crystal to stabilize regular colloidal structures is one of the key issues for possible use of nematic colloids in photonic applications [13].

II. MODELING

Dispersion of colloidal particles in a thin layer of nematic phase is an example of complex confinement. Nematic is affected by surfaces confining the layer and by surfaces of the colloidal particles (Fig. 1).

In addition, the particles are free to move under the action of the thermodynamic forces, driving the system toward the state of minimal free energy. Our system is characterized by scales ranging from few nanometers to few micrometers. In this case, a phenomenological description of nematic phases based on the order parameter [1,14], is the best tool for studying colloidal structures. It is essential to use the full order parameter tensor Q_{ij} [15], which includes director $\boldsymbol{n}$, scalar order parameter S, and biaxiality η:

$$Q_{ij} = S/(3n_i n_j - \delta_{ij})2 + \eta/(e_i^{(1)} e_j^{(1)} - e_i^{(2)} e_j^{(2)})2, \tag{1}$$

where $e_i^{(1)}$ are components of the secondary director (corresponds to the second largest eigenvalue of Q_{ij}) and $\boldsymbol{e}^{(2)} = \boldsymbol{n} \times \boldsymbol{e}^{(1)}$.

Using the complete order parameter tensor proves to be crucial when modeling the ordering of nematic colloidal systems, as frustration caused by complex geometries of confining surfaces or opposing surface anchorings give rise to formation of defects (regions where the director field is discontinuous), while S and η exhibit strong but continuous variation. Using Landau-de Gennes approach [1,14] a free energy composed of elastic, ordering, and surface contributions is constructed:

$$F = \int_{LC} f_e \, dV + \int_{LC} f_{ord} \, dV + \int_{Surf.Col.} f_s \, dS \tag{2}$$

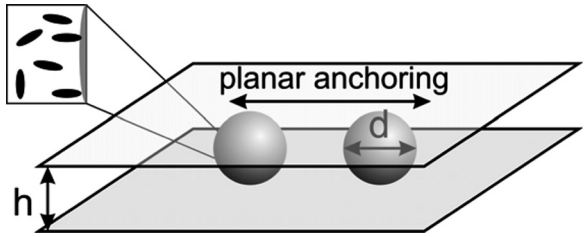

FIGURE 1 Schematic presentation of a thin nematic layer with dispersed colloidal particles. Thickness h is comparable to particle diameter d.

For the volume density of elastic free energy f_e we choose the simplest single elastic constant (L) form:

$$f_e = \frac{1}{2}L\left(\frac{\partial Q_{ij}}{\partial x_k}\right)\left(\frac{\partial Q_{ij}}{\partial x_k}\right). \tag{3}$$

This simplifies the calculations but allows only qualitative predictions. For the simplest phase free energy density that describes the degree of ordering [1,14]

$$f_{ord} = \frac{1}{2}AQ_{ij}Q_{ji} + \frac{1}{3}BQ_{ij}Q_{jk}Q_{ki} + \frac{1}{4}C\left(Q_{ij}Q_{ji}\right)^2, \tag{4}$$

we need three material constants: A, B, and C. For the surface free energy density we choose "Rapini-Papoular"-like form [16]

$$f_s = \frac{1}{2}W(Q_{ij} - Q^0_{ij})(Q_{ji} - Q^0_{ji}), \tag{5}$$

characterized by the surface anchoring strength W and the preferential surface order parameter tensor Q^0_{ij}. Note that summation over repeated indices is assumed.

In order to obtain the equilibrium order parameter tensor profile and particle distribution, F, the total free energy of a confined nematic, is minimized with respect to ordering tensor field and particle positions. Minimizing according to Euler–Lagrange formalism yields a set of six partial differential equations.

$$0 = L\nabla^2 Q_{ij} - AQ_{ij} - BQ_{ik}Q_{kj} - CQ_{ij}(Q_{kl}Q_{lk}) \tag{6a}$$

$$0 = L\nu_k \partial Q_{ij}/\partial x_k + W(Q_{ij} - Q^0_{ij}). \tag{6b}$$

ν_k is the surface normal. Equations were solved numerically by an explicit relaxation algorithm on a cubic mesh [17]. The mesh points, where calculations are performed, are divided into three categories. This is done in order to account for the surface interaction of particles with the bulk nematic liquid crystal. The categories are: bulk nematic points that obey bulk nematic equations, interfacial points (surface layer) that obey surface equations, and colloid points where nematic is not present. Schematic picture of a two-dimensional cross-section through a spherical colloid is visualized in Figure 2. Interfaces are in this manner described as shells of the thickness determined by the mesh resolution (i.e., 10 nm).

Strong unidirectional planar anchoring is assumed for both planar surfaces that confine our nematic slab. The resulting boundary

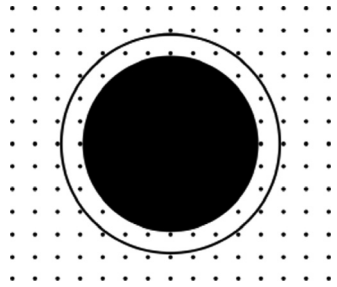

FIGURE 2 Schematic picture of a colloidal particle positioned inside a numerical mesh (black dots). Tensorial field at mesh points within the bulk region obeys bulk equations, while at surface points in the interfacial region the surface equations are satisfied.

condition is thus characterized by the fixed order parameter tensor field corresponding to the perfectly oriented nematic. In all presented calculations (if not stated otherwise) the following parameter values have been used: 2 μm layer thickness, 1 μm particle diameter d, $A = -0.172\,\mathrm{MJ/m^3}, B = -2.12\,\mathrm{MJ/m^3}, C = 1.73\,\mathrm{MJ/m^3}, L = 4 \times 10^{-11}\,\mathrm{N}$, and very strong anchoring strength $W = 10^{-2}\ \mathrm{J/m^2}$. The preferential particle surface order parameter tensor was chosen to be uniaxial with its primary axis being perpendicular to the particle surfaces and the degree of order being equal to the equilibrium bulk value. The choice of material parameters, that corresponds to a 5CB liquid crystal with the bulk scalar order parameter $S_0 = 0.533$ yields the nematic correlation length $\xi_N = [3L/(3A + 3BS_o + 27CS_o^2/2)]^{1/2} = 6.63\,\mathrm{nm}$ [1,14]. The value of the ξ_N dictated our selection of the resolution characterized by 10 nm lattice constant of our mesh. With number of points being typically few times 10^2 in each of x, y and z directions, the total number of mesh points often reaches 10^7.

The use of a relaxation algorithm to solve the Euler-Lagrange equilibrium equations mimics the time evolution of the investigated nematic ordering field. The description incorporates only one effective rotational nematic viscosity and neglects effects of material flows. As a consequence of these omissions, it is only qualitative. In complex nematic confinements there are usually several metatastable structures that are close in energy, but separated by pronounced energy barriers. The relaxation can lead to different final states, depending on initial conditions. This actually proves to be the key element in the creation of entangled defect structures. Homogeneous initial configuration strongly suppresses formation of extended defects as it "allows" formation of defects only close to the colloidal particle

surfaces yielding either dipolar or quadrupole structures. However, if the initial configuration is random, defects start forming everywhere in the bulk of the liquid crystal. Thus, a large number of them is generated right at the beginning of the relaxation process. As the relaxation process proceeds, the majority of these defects annihilates or disappears. However, some of them can get entangled and pinned to colloidal particles although they may be metastable. When an experiment is performed, the relaxation, following an isotropic to nematic quench, closely resembles the behavior predicted by our simplified numerical procedure [11].

III. RESULTS AND DISCUSSION

Monomers and 'regular' Dimers

Colloidal particles with homeotropic surface anchoring, placed in a thin nematic liquid crystal layer (confined by two surfaces inducing strong parallel planar anchoring), are characterized by two specific nematic configurations: an elastic dipole and an elastic quadrupole (Saturn ring configuration). These are structures well known from the literature [3] and can be interpreted through the analogy of the director field profile with the electrostatic potential.

At this point, we can also touch upon the topological aspects. Each particle with the homeotropic surface anchoring is equivalent to a defect with topological charge one. A sign of plus one is associated with this structure, called the radial hedgehog structure [1]. Confining such an object into a thin layer of a nematic liquid crystal, where surface enforces homogenous nematic field, a defect is formed. This defect has the opposite topological charge to that of a particle, yielding the structure with total charge zero. This defect having charge -1 is in fact a disclination loop characterized by winding number $-1/2$. In the dipolar case the loop has nanometer scale and is usually called hyperbolic hedgehog. In the quadrupole case the $-1/2$ disclination loop has Saturn ring shape and a scale comparable to the particle diameter. In Figure 3, we visualize calculated dipolar and quadrupolar nematic configurations. The dipole structure is stable in case of weak confinement and quadrupole in case of strong confinement. When the layer thickness is comparable to the particle diameter free energies of both structures are comparable and structures can coexist although one is stable and the other is metastable. One can affect stability also by changing anchoring strength or applying external field.

When assembling colloidal particles with the intention of building multi-particle colloidal structures, one should first start with colloidal

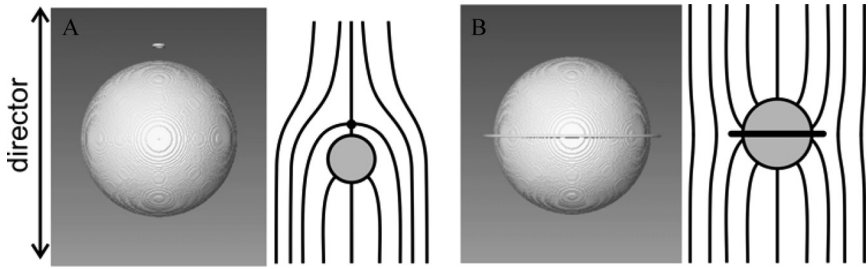

FIGURE 3 Nematic configurations around homeotropic colloidal particles in a nematic cell with planar anchoring. Nematic structures characterized by disclination loops are visualized both by calculated isosurfaces of the scalar order parameter $S = 0.45$ ($S_{bulk} = 0.533$) and by a schematic presentation of the director field lines: (A) elastic dipole and (B) elastic quadrupole (Saturn ring structure). In calculations the particle diameter was 2 μm and layer thickness 2.5 μm.

dimers. Two elastic dipoles can assemble either in a parallel or anti-parallel way with respect to their defect positions. Parallel dipoles form chains and the anti-parallel dipoles form a more complicated tilted configuration. Both equilibrium particle configurations with corresponding disclination loops are presented in Figure 4A and B, together with the corresponding schematic picture of the director field profiles. Note the tilt of dipoles in the anti-parallel configuration and the alignment of the dimer with parallel dipoles along the director. Two quadrupolar particles have only one positional equilibrium configuration, where they bind in a side-by-side way at an angle of $\sim 73^\circ$ with respect to the far-field director. The equilibrium configuration of a quadrupolar dimer is presented in Figure 4C. For mixed assemblies of dipolar and quadrupolar structures see reference [18].

Entangled Dimers

Primary target of this short review are nematic braids. Nematic braids are structures where colloidal particles are entangled by disclination lines. Such entangled structures are easily formed after isotropic-nematic quench in a thin layer if the particles are close enough. This was not recognised until recently, when they were first predicted theoretically and then realized in experiments [9,11,19]. These structures typically have higher total free energies than those of either dipoles or quadrupoles and are thus metastable. Three different metastable entangled dimer structures have been observed and are visualized in Figure 5: figure of eight (A), figure of omega (B), and entangled hyperbolic defect structure (C). In the figure of eight configuration, a

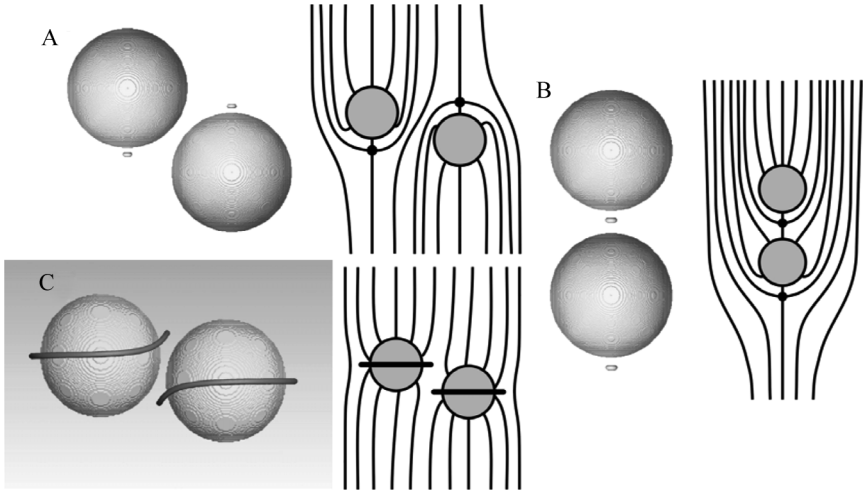

FIGURE 4 Nematic configurations around dimers formed by two homeotropic colloidal particles in a nematic cell with planar anchoring. Nematic structures are visualized both by calculated isosurfaces of the scalar order parameter $S = 0.45$ ($S_{bulk} = 0.533$) and by a schematic presentation of the director field lines: (A) two antiparallel elastic dipoles, (B) two parallel elastic dipoles, and (C) two side-by-side elastic quadrupoles. (Saturn ring structures). In (A) and (B) the particle diameter was 2 μm and layer thickness 2.5 μm.

single $-1/2$ defect line winds around two particles starting at one side of the first particle, dropping below the second particle, coming from the back to the top of the second particle, and finally sinking below the first particle. In the figure of omega configuration again a single

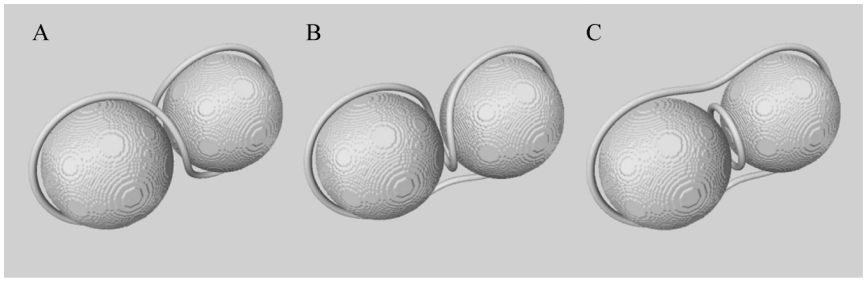

FIGURE 5 Calculated structures of entangled nematic colloidal dimers where cores of the disclination loops are visualized by isosurfaces of the scalar order parameter being $S = 0.45$ ($S_{bulk} = 0.533$). (A) figure of eight defect structure, (B) figure of omega defect structure, and (C) entangled hyperbolic defect structure.

$-1/2$ defect line winds around the two particles and makes an omega like loop between the particles. Formation of A and B loops also breaks inversion symmetry. The structures with left or right chirality are equally probable. In the entangled hyperbolic defect structure two separate perpendicular $-1/2$ defect loops are involved. The first larger loop encircles both particles at their equator, while the second, smaller loop is a ring (in principle a hyperbolic -1 point defect) that sits between the two particles in a 'classical dipolar manner'. This structure was probably obtained earlier in the simulations of nanocolloids but was never fully explained [15].

Let us consider how the topological condition requiring zero total topological charge is satisfied. In the C case we have two $-1/2$ disclination loops each caring topological charge -1 that exactly compensates two $+1$ charges of colloidal particles. In A and B cases where a single disclination loop entangles both particles, it is clear that it must carry charge -2. These loops differ from the one in the C case only in the twisted regions, clearly suggesting that additional charge comes from the twist. Using the well known expression for the calculation of the topological charge [1]

$$q = (1/4\pi) \iint du dv \quad \boldsymbol{n} \cdot (\partial \boldsymbol{n}/\partial u \times \partial \boldsymbol{n}/\partial v) \tag{7}$$

where integration is performed over a closed surface (parametrised by coordinates u and v), incorporating the loop. One can check the total charge of the twisted loops.

The free energy estimates based on our single elastic constant Landau de Gennes approach indicate that all three entangled colloidal pairs are metastable with 0.3% (figure of eight), 0.9% (figure of omega) and 0.7% (entangled hyperbolic defect) higher free energy than the free energy of a bound quadrupolar pair. Nevertheless, there is an important difference that makes the above metastable structures far more robust than the dipolar or quadrupolar pairs. The important difference between entangled and non-entangled structures is the stretching of the disclination lines. The coupling of particles by the disclination loop resembles that of a string. The force is practically independent of distance a consequence the energy being approximately proportional to the length of the disclination loops. On the other hand, in both non-entangled cases the effective inter-particle force is even slightly stronger close to equilibrium distances but strongly decays with further increase of the distance. The robust coupling of the colloids by the disclination loops makes entangled colloidal dimers new basic building blocks for more complex nematic braids.

Entangled Colloidal Chains

Formation of chains based on dipolar and quadrupolar dimers are well known [2]. Here we are interested in entangled chains. Modeling predicts chains based on all three entangled dimer structures. See Figure 6A and B where chains based on the figure of eight dimer and entangled hyperbolic point defect structure are illustrated. Experimental formation of entangled chains is more complicated as one must "glue" together two dimmers by "melting" only the intermediate region. Nevertheless, it confirms predictions [11]. In numerical calculations, the right initial conditions have to be chosen to generate particular defect structures. Typically, periodic boundary conditions are chosen in the direction of chains, with the unit cell of one or two particles. If the structure has a finite number of colloids (N), the line that entangles colloids on both ends closes and forms a single loop – topological object – that has charge $-N$ in the case of the "figure of eight" based structures and charge -1 in the case of

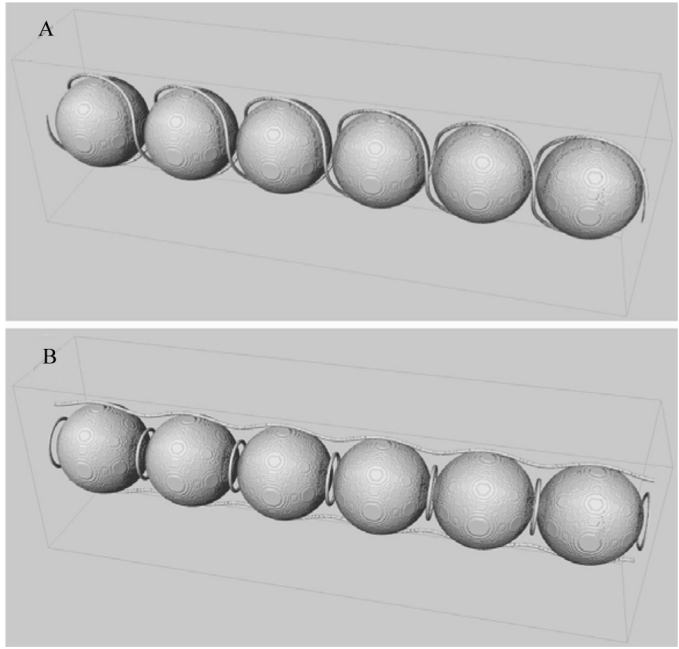

FIGURE 6 Colloidal chains where the cores of the disclination loops are visualized by isosurfaces of the scalar order parameter being $S = 0.45$ ($S_{bulk} = 0.533$): (A) figure of eights chain, (B) entangled hyperbolic defects chain.

N−1 entangled hyperbolic defects linking N particles. Finally, it should be stressed that both structures are oriented perpendicularly to the director enforced by the confining surfaces.

Hierarchical Self-Assembly of Colloidal Superstructures

Here we briefly review our recent study [12] where we show that various colloidal superstructures could be hierarchically self-assembled in nematic colloids of different sizes using topological and elastic properties of nematic solvents. For a small particle in a nematic liquid crystal with disclination lines, it is energetically more favorable to migrate into the core of these lines [20,21]. The driving mechanism is the minimization of the total nematic free energy. Applying this principle to nematic colloids, where one can form dislination network with nearly arbitrary complexity it is possible to realize the self assembly of complex multiscale colloidal structures. Here we illustrate trapping of small particles into the Saturn ring disclination (Fig. 7A,B). Experimental studies confirmed the assembly procedure and show that it works also in more complex cases. Trapping of small particles is limited by their anchoring strength and size. For instance in the case of strong anchoring ($10^{-3}\,\mathrm{Jm}^{-2}$) particles down to 40 nm diameter can be trapped in the Saturn ring disclination of a particle with diameter 1 micrometer [12].

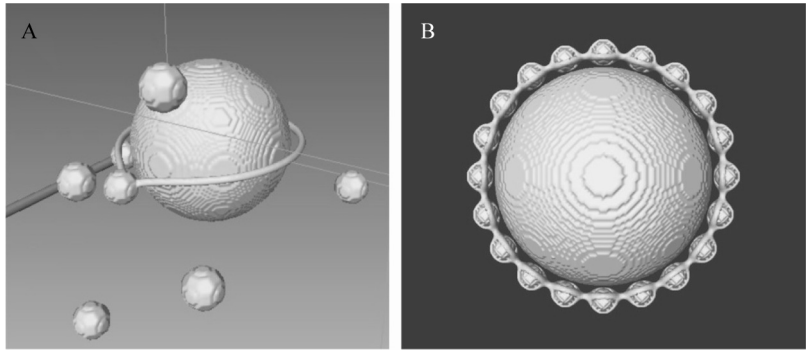

FIGURE 7 Hierarchical superstructure formed of small colloidal particles trapped into the Saturn ring of the large particle. Cores of the disclination loops are visualized by isosurfaces of the scalar order parameter being $S = 0.45$ ($S_{bulk} = 0.533$). (A) Trapping of small particles in the Saturn ring formed around a large colloidal particle. (B) Equilibrium superstructure where Saturn ring of a large 1 μm particle is decorated by small 100 nm colloidal particles.

IV. CONCLUSION

Unlike forces that are responsible for the organization of colloidal particles in simple solvents, the structural forces in the nematic colloids are anisotropic and can act on hierarchically chosen length scales originating from the intrinsic particle scales and anchoring strengths. This allows us to assemble predetermined colloidal superstructures ranging from micrometer to nanometer scale. Modeling of the assembling process is crucial for understanding and design of nematic colloidal structures. In this brief review we have started from simple homeotropic particles characterized by dipolar and quadrupolar configurations of the nematic liquid crystal around the colloids. We have explained the assembly of entangled structures using the arguments of topology and further demonstrated that dimer structures can be extended to linear and also to hierarchical configurations.

The strong binding of entangled colloidal particles together with possible fuctionalization of particles opens new routes to possible applications, such as beam steering, controllable photonic bad-gap colloidal structures, plasmonics and metamaterials [22].

REFERENCES

[1] Kleman, M. & Lavrentovich, O. D. (2006). *Soft Matter Physics: An Introduction*, Springer: New York.
[2] Poulin, P., Stark, H., Lubensky, T. C., & Weitz, D. A.. (1997). *Science*, *275*, 1770.
[3] Stark, H. (2001). *Phys. Rep.*, *351*, 387.
[4] Smalyukh, I. I., Lavrentovich, O. D., Kuzmin, A. N., Kachynski, A.V., & Prasad, P. N. (2005). *Phys. Rev. Lett.*, *95*, 157801.
[5] Kotar, J., Vilfan, M., Osterman, N., Babič, D., Copič, M., & Poberaj, I. (2006). *Phys. Rev. Lett.*, *95*, 207801.
[6] Loudet, J. C., Barois, P., & Poulin, P. (2000). *Nature*, *407*, 611.
[7] Poulin, P. & Weitz, D. A. (1998). *Phys. Rev.*, *E 57*, 626.
[8] Nazarenko, V. G., Nych, A. B., & Lev, B. I. (2001). *Phys. Rev. Lett.*, *87*, 075504.
[9] Muševič, I., Škarabot, M., Tkalec, U., Ravnik, M., & Žumer, S. (2006). *Science*, *313*, 954.
[10] Žumer, S. (July 2–7, 2006). *plenary talk at 21st International Liquid Crystal Conference*, Keystone, Colorado.
[11] Ravnik, M., Škarabot, M., Žumer, S., Tkalec, U., Poberaj, I., Babič, D., Osterman, N., & Muševič, I. (2007). *Phys. Rev. Lett.*, *99*, 247801.
[12] Škarabot, M., Ravnik, M., Žumer, S., Tkalec, U., Poberaj, I., Babič, D., & Muševič, I. (2008). *Phys. Rev.*, *E 77*, 061706.
[13] Muševič, I. & Škarabot, M. (2008). *Soft Matter.*, *4*, 195–199.
[14] de Gennes, P. G. & Prost, J. (1993). *The Physics of Liquid Crystals,* 2nd ed., Oxford Science Publications: Oxford.
[15] Guzman, O., Kim, E. B., Grollau, S., Abbott, N. L., & de Pablo, J. J. (2003). *Phys. Rev. Lett.*, *91*, 2355207.
[16] Fournier, J. B. & Galatola, P. (2005). *Europhys. Lett.*, *72*, 403409.

[17] Press, W. H., Flannery, B. P., Teukolsky, S. A., & Vetterling, W. T. (1986). *Numerical Recipies*, Cambridge University Press, Cambridge.
[18] Ognysta, U., Nych, A., Nazarenko, V., Muševic, I., Škarabot, M., Ravnik, M., Žumer, S., Poberaj, I., & Babič, D. (2008). *Phys. Rev. Lett.*, *100*, 217803.
[19] Araki, T. & Tanaka, H. (2006). *Phys. Rev. Lett.*, *97*, 127801.
[20] Pires, D., Fleury, J.-B., & Galerne, Y. (2007). *Phys. Rev. Lett.*, *98*, 247801.
[21] Antypov, D. & Cleaver, D. J. (2004). *J. Phys.: Condens. Matter*, *16*, S1887.
[22] Shelby, R. A., Smith, D. R., & Schultz, S. (2001). *Science*, *292*, 77–79.